Boletim da Sociedade Astronômica Brasileira, **35**, no. 1, 167-171

Compact object populations over cosmic time

L. M. de Sá[1], A. Bernardo[1], R. R. A. Bachega[1], L. S. Rocha[1,2], & J. E. Horvath[1]

[1] Instituto de Astronomia, Geofísica e Ciências Atmosféricas, Universidade de São Paulo, Rua do Matão, 1228, Butantã, São Paulo, Brasil e-mail: lucasmdesa@usp.br
[2] Instituto de Física, Universidade de São Paulo, Rua do Matão, 1371, Butantã, São Paulo, Brasil

Abstract. Over the past few years, the steadily growing catalog of compact object mergers observed by the LVK Collaboration has allowed for the construction of a population picture of these events as a population to start to emerge. One invaluable tool in the exploitation of this growing catalog has been rapid binary population synthesis (BPS), which allows for predicting the rate of observed mergers and their properties, whilst also constraining the initial conditions of stellar/binary formation and evolutionary models by comparing the results with observations. While much has been done in BPS to constrain the evolutionary models, the initial conditions have been relatively neglected. Chiefly, this ignores the long-expected trend of the initial mass function (IMF) to become top-heavy at higher redshifts, i.e., to produce more compact object progenitors. One such model for a varying IMF is the integrated-galaxy wide IMF (IGIMF). In this work, we employ the IGIMF and correlated orbital parameter distributions to perform the population synthesis of compact object mergers with the COMPAS code. We generated populations consistent with star formation rate, metallicity and IMF evolution with redshift, and studied how observed merger rates and other properties vary with redshift. We find an overall tendency of merging binaries to be more massive the older they are and the higher the merger redshift is. We also find evidence for a peak in the merger rate of binary black holes (BBHs) between redshifts ~ 2 and ~ 1. As further improvements are made to current gravitational observatories and we reach their next generation, merger observations will begin to regularly probe the $\gtrsim 1$ redshift region, where we expect different star formation conditions to play a significant role in variations of the merger population. Our work provides a framework for redshift-dependent population synthesis broadly speaking, and tests a particular varying IMF.

Resumo. Ao longo dos últimos anos, o crescente catálogo de fusões de objetos compactos observadas pela Colaboração LVK tem permitido a construção de uma imagem da população desses eventos. Uma ferramenta valiosa na exploração deste crescente catálogo tem sido a síntese de populações binárias (BPS) rápida, que permite predições da taxa de fusões observadas e suas propriedades, e também estabelece vínculos para as condições iniciais de formação estelar/binária e modelos evolutivos atrvés da comparação dos resultados com observações. Enquanto muito tem sido feito com a BPS para limitar os modelos evolutivos, as condições iniciais têm sido relativemente negligenciadas. Sobretudo, isto ignora a tendência há muito tempo esperada de que a função de massa inicial (IMF) torne-se *top-heavy* em altos redshifts, i.e., produza mais progenitoras de objetos compactos. Um exemplo de modelo para uma IMF variante é a *integrated galaxy-wide IMF* (IGIMF). Neste trabalho, nós empregamos a IGIMF e disitribuições correlacionadas de parâmetros orbitais para realizar a síntese populacional de fusões de objetos compactos com o código COMPAS. Com isto, nós geramos populações consistentes com a taxa de formação estelar, metalicidade e evolução da IMF sobre redshift, e estudamos como taxas de fusão observadas e outras propriedades variam com o redshift. Nós encontramos uma tendência geral de binárias fusionantes serem tão mais massivas quanto mais velhas forem e quão mais alto o redshift de fusão for. Também encontramos evidência de um pico na taxa de fusão de buracos negros binários (BBHs) entre redshifts ~ 2 e ~ 3. Conforme melhoras são realizadas sobre observatórios gravitacionais atuais e alcançamos a sua próxima geração, observações de fusões começarão a explorar regularmente a região $z \gtrsim 1$, onde esperamos que condições de formação estelar diferentes tenham um papel significante em variações da população de fusões. Nosso trabalho oferece uma estrutura para síntese de populações depedente de redshift de forma geral, e testa uma IMF variante particular.

Keywords. Stars: neutron – Binaries: close – Gravitational waves

1. Introduction

One of the main tools for studying binary compact object (BCO) populations are rapid binary population synthesis (BPS) codes. BPS codes approximate the evolution of isolated binaries by means of simple prescriptions based on detailed simulations, starting from the conditions of star formation, making possible the synthesis of much larger populations than would be otherwise. These codes allow not only estimating properties of BCO populations, but also testing evolution and initial condition models against empirical constraints, such as measured BCO merger rates (Abbott et al. LIGO-Virgo-KAGRA Collaboration, 2021).

The exploration of such constraints has so far focused mostly on variations of the stellar/binary evolution models, such as those for the common envelope phase or supernova remnant mass prescriptions (e.g., Broekgaarden et al. 2021). The initial conditions, i.e., property distributions for zero age-main sequence (ZAMS) stars and binaries, in contrast, have received relatively less attention (albeit some works, such as Klencki et al. 2018, have begun to tackle the issue recently). Possible correlations between orbital parameters, for example, are usually not taken into account; and the long-standing issue of variations of the initial mass function (IMF) with respect to metallicity and the local star formation rate (SFR) (see, e.g., Hopkins 2018), with potential implications for BCOs, is also usually left out.

In our work, we have sought to provide an expressive refinement of the treatment given to initial conditions in BPS, by implementing in the open-source COMPAS BPS code (Team COMPAS: Riley et al. 2022) both a varying IMF and correlated orbital parameters in generating binary populations formed over the entire span of cosmic star formation history (SFH), in order to evaluate how compact object populations, particularly those of compact binary mergers (CBMs), might vary over cosmic

time. Here we briefly describe the models involved, and present some of the results we have obtained.

2. Distributions for initial sampling

The main "ingredient" for our initial sampling is the IMF. Here, we have as a baseline model the Kroupa (2001) IMF, a two-part power law with index -1.3 between 0.08 and 0.5 $M_\odot$ and -2.3 (the Salpeter 1955, index) between 0.5 and 150 $M_\odot$; we refer to this as the "canonical" IMF. For modeling variations of the IMF, we adopt the model by Jeřábková et al. (2018). Their *galactic* IMF (gIMF, ξ_g), i.e., for the population of an entire galaxy, is built within the framework of integrated galaxy-wide IMF theory (or IGIMF, originally by Kroupa & Weidner 2003), wherein star formation is considered to take place within individual *embedded clusters* (ECLs), each of which has its own associated *stellar* IMF (sIMF, ξ_s), whereas the ECLs themselves are distributed according to their own IMF (eIMF, ξ_e); the gIMF then emerges as the integration over the sIMF of all ECLs. If the sIMF is allowed to vary from cluster to cluster, then each galaxy may have a different gIMF depending on its eIMF.

The implementation of IGIMF theory by Jeřábková et al. (2018) is based on two empirical fits: one for the sIMF, by Marks et al. (2012), who found a tendency of the IMF to become top-heavy and bottom-light at lower metallicities; and the other for the eIMF, by Gunawardhana et al. (2011), who found a tendency of the IMF to become top-heavy in galaxies with high SFR. Thus, they obtain a gIMF dependent on the metallicity and SFR of the environment, as

$$\xi_g(m|\,[\mathrm{Fe/H}]\,,\mathrm{SFR}) = \int_5^{10^9} \xi_s\,(m|[\mathrm{Fe/H}]\,,\mathrm{SFR})\;\xi_e\,(M_{ecl}|\mathrm{SFR})\;\frac{\mathrm{d}M}{M_\odot}, \quad (1)$$

a few examples of which are shown in Fig. 1. We refer to this as the "varying" IMF.

The second ingredient are the distributions for the orbital parameters: the orbital period, P (usually drawn as $\log P$); the mass ratio between primary (m_1) and companion (m_2) mass, $q = m_2/m_1 \leq 1$; and the eccentricity, $e = 0$. Here, the usual "canonical" distributions are: a uniform distribution between 0.01 and 1 for the mass ratio (Sana et al. 2012); a log-uniform distribution between $10^{0.4}$ and 10^3 days for the orbital period (Öpik 1924); and initially circular orbits ($e = 0$). On the other hand, Moe & Di Stefano (2017) more recently fitted series of power law and linear distributions for all three quantities from a large sample of observed binaries from a variety of sources, each corrected for its own selection effects, and found all of them to be correlated: $\log P$ to m_1; and q and e to both m_1 and $\log P$. As the authors discuss, these correlations are likely consequences of pre-zero age main sequence (ZAMS) evolution, and tend to, for example, drive binaries with shorter periods towards more symmetrical masses and less eccentric orbits. We also include these distributions in the generation of our initial samples. We refer to these as the "correlated" orbital parameter distributions.

Since for the orbital period Moe & Di Stefano (2017) fit the *companion frequency* as function of orbital period (and primary mass), this also constrains the binary fraction as a function of m_1. We follow the authors' suggested method of computing the binary fraction from the companion frequency, which we discuss in detail in de Sá et al. (in preparation).

The third and last ingredient concerns environmental conditions, which, in our case, are the metallicity and SFR. Here we employ the cosmic SFH computed by Chruślińska, Nelemans & Belczynski (2019) for a set of 24 possible combinations between different models for the galaxy stellar mass function (GSMF), mass-metallicity relation (MZR) and star formation-mass relation (SFMR); corrections to the SFR measurements involved, made assuming a Kroupa (2001) IMF, for the Jeřábková et al. (2018) IMF were computed by Chruślińska et al. (2020). For all results presented here we adopt the "moderate metallicity" model defined in Chruślińska, Nelemans & Belczynski (2019), shown in Fig. 2, in the Jeřábková et al. (2018) IMF case, as a cosmic stellar mass distribution over metallicity and SFR, which can in practice be employed as a probability distribution for both of these variables.

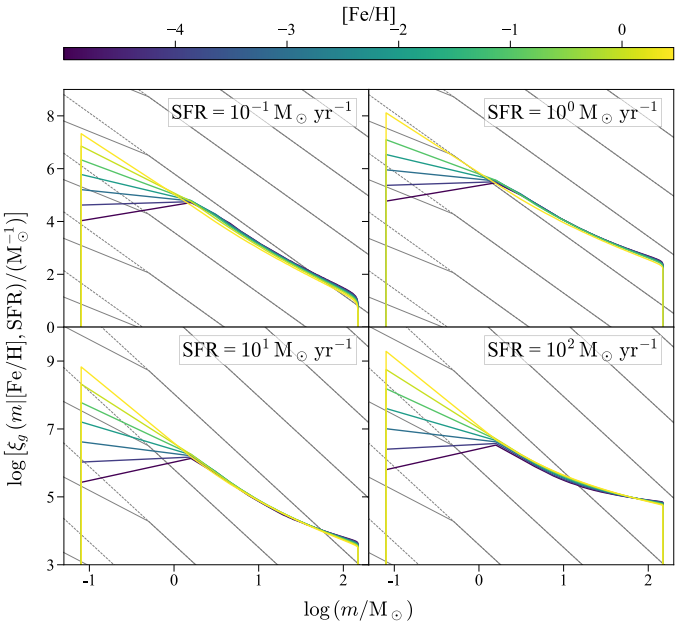

Figure 1. The varying gIMF from Jeřábková et al. (2018) computed for different pairs of metallicity and SFR (solid colored lines); and the Kroupa (2001) (solid black lines) and Salpeter (1955) (dashed black lines) IMFs for reference. For higher SFRs, the varying IMF tends to become strongly top-heavy; while for low metallicities, it tends to become strongly bottom-light and slightly top-heavy.

These three "ingredients" are used in building our initial sample as a *composite* binary population, composed of simple populations sampled on the SFR-metallicity plane in such a way that reproduces, within the resolution of the sample, the cosmic SFH, as illustrated in Fig. 2. Then, for each simple population we draw our binaries, each defined by its $(m_1, q, \log P, e)$.

We build our samples by drawing 10 redshifts between $z = 0$ and $z = 10$ (assumed start of star formation), and manually including $z = 0.01$ and $z = 10$ as boundary conditions. For each redshift we sample 10 metallicities, resulting in 120 simple populations, for each of which we draw $\sim 10^6$ binaries; thus each of our initial samples contains $\sim 10^8$ binaries, only a small fraction of which will evolve into CBMs. At the moment we compare two such samples: one evolved with the "IGIMF" model (varying IMF and correlated orbital parameter distributions), and one for the "Canonical" model (canonical IMF and orbital parameter distributions). Both are evolved with `COMPAS` in its default settings for 13.8 Gyr, and finally we separate the resulting BCOs that have had time to merge when taking into account their age (i.e., initial redshift). Below we examine some results in both the IGIMF and Canonical models, focusing on the largest por-

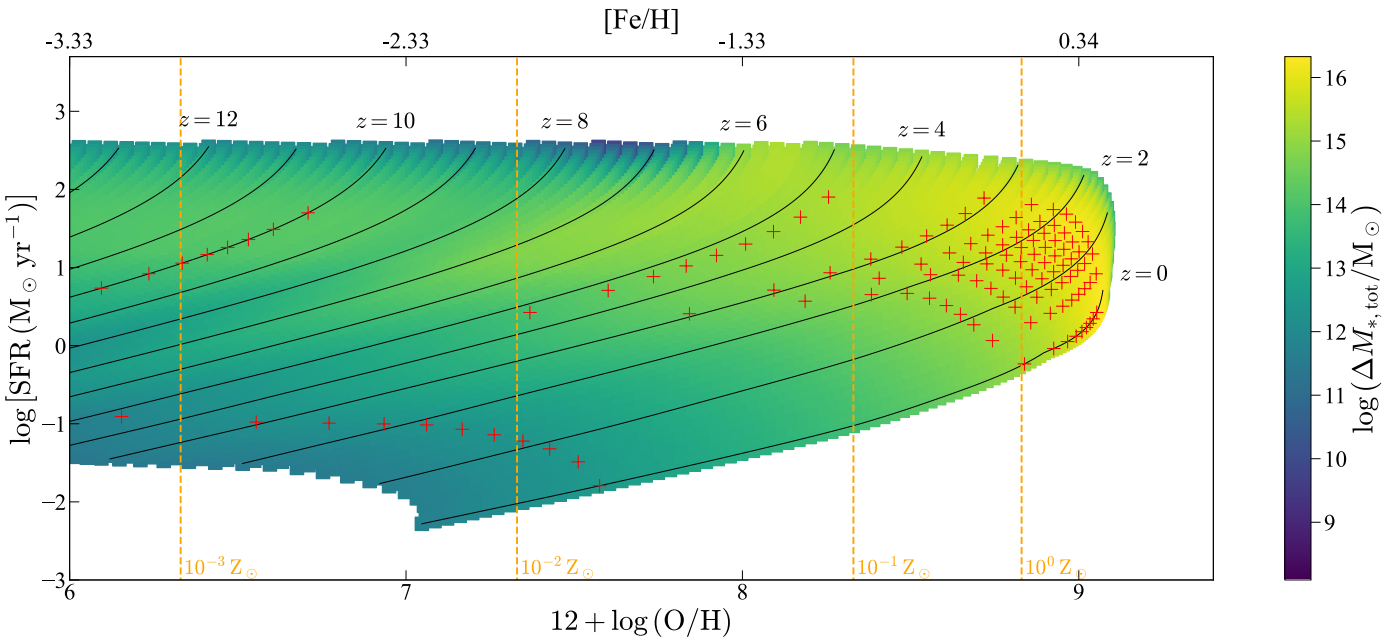

Figure 2. Cosmic SFH computed in the moderate (fiducial) metallicity model from Chruślińska, Nelemans & Belczynski (2019), with corrections for the Jeřábková et al. (2018) IMF by Chruślińska et al. (2020), for star-forming galaxies between 10^6 and $10^{12}\,M_\odot$. The color plot displays the total stellar mass formed at different configurations of SFR and metallicity, while the black solid lines are lines of constant redshift; thus the temporal evolution of star formation occurs from left to right. The orange dashed lines indicate metallicity in units of Solar metallicity. In practice, the mass distribution allows us to choose our simple populations in a way that is representative of the cosmic SFH. The red crosses show the result of the sampling for 10 redshifts between 0 and 10, and 10 metallicities per redshift. The $z > 10$ region is only included to exemplify a extrapolation of the models.

tion of the BCM sample, that of black hole-black hole (BHBH) mergers.

3. Results for merger rates and BHBH masses

Of the $\sim 10^8$ initial binaries, only $\approx 1.9 \times 10^5$ evolve up to a BHBH merger within the available time; the number for black hole-neutron star (BHNS) mergers is an order of magnitude lower; and, for neutron star-neutron star mergers (NSNS), two orders of magnitude lower. This in itself already reproduces the observed rarity of NSNS mergers, which goes against old expectations that they should be more common due to the relative abundance of NS progenitors. The main property of individual mergers that we can track over redshift are the masses, which we discuss below.

We distinguish between two redshifts associated to each system: the redshift of formation, z_{ZAMS}, and the redshift at merger, z_{merger}. While z_{merger} is an observable, z_{ZAMS} must be understood as the redshift at which we currently observe the Universe at the age in which the system was formed, but not its formation itself. With that in mind, we can track both the evolution of BHBH component masses with regard to z_{merger} and examine the contribution of populations of different ages through z_{ZAMS}. Therefore we focus on the evolution with z_{merger}.

In Figs. 3 and 4 we show the primary mass distribution (most massive component) for different z_{merger}, for the Canonical and IGIMF models, respectively. Key features are the peaks at ~ 9, ~ 16 and $\sim 45\,M_\odot$. In the IGIMF model (Fig. 4) there is a clear shift from the ~ 9 to the $\sim 16\,M_\odot$ peak as redshift increases, with the first becoming dominant for $z_{\mathrm{merger}} \lesssim 2$; as well as the presence of the $\sim 45\,M_\odot$ peak at the highest redshifts ($z_{\mathrm{merger}} \gtrsim 4$). In the Canonical model the $\sim 16\,M_\odot$ peak is always dominant, but there is an evident shift of the distribution towards the lower peak as the redshift decreases. We see thus a tendency of the mass to increase with redshift in BHBH mergers; primary BHs with $\lesssim 12\,M_\odot$ in particular are predominantly found in $z_{\mathrm{merger}} \lesssim 2$.

While the initial conditions dictate the weight of each peak, their *location* is a consequence of particular formation channels for BCMs. The $\sim 45\,M_\odot$ peak is a direct result of the default pulsation pair-instability supernovae (PPINSe) model in `COMPAS` (by Marchant et al. (2019), as implemented by Stevenson et al. (2019)). A similar work with `COMPAS` by van Son et al. (2022a) found a characteristic peak around $\sim 18\,M_\odot$ due to the (dominant) common envelope (CE) formation channel, in which the companion starts a common envelope (CE) phase after the primary has already collapsed. The rarer channel of stable Roche lobe overflow (RLOF) onto the collapsed primary produces the peak at $\sim 9\,M_\odot$ (van Son et al. 2022b). The IGIMF model thus tends to increase the likelihood of formation through the stable RLOF channel considerably at low redshift; it remains for us to separately test the varying IMF and the correlated orbital parameter distributions in order to evaluate their individual roles in giving rise to this behavior.

We also find a peak at $\sim 30\,M_\odot$ for lower redshifts in both cases. It is worth noting that an overdensity centered on $35\,M_\odot$ was found in the GWTC-3 BHBH primary mass distribution by Abbott et al. (LIGO-Virgo-KAGRA Collaboration, 2021), overlaid on a power-law distribution with peak at $\sim 9\,M_\odot$; this is similar to the shape obtained from the IGIMF model, but not the Canonical one. van Son et al. (2022a) point out that, in the particular case of `COMPAS`, this $\sim 30\,M_\odot$ peak is an artifact from the transition between remnant masses originating directly from core-collapse supernovae (CCSNe) (Fryer et al. 2012) and those from stars that underwent PPISN mass loss before core-collapse; but it is also not clear that the transition between CCSNe and PPISNe should be smooth in Nature. However, van Son et al.

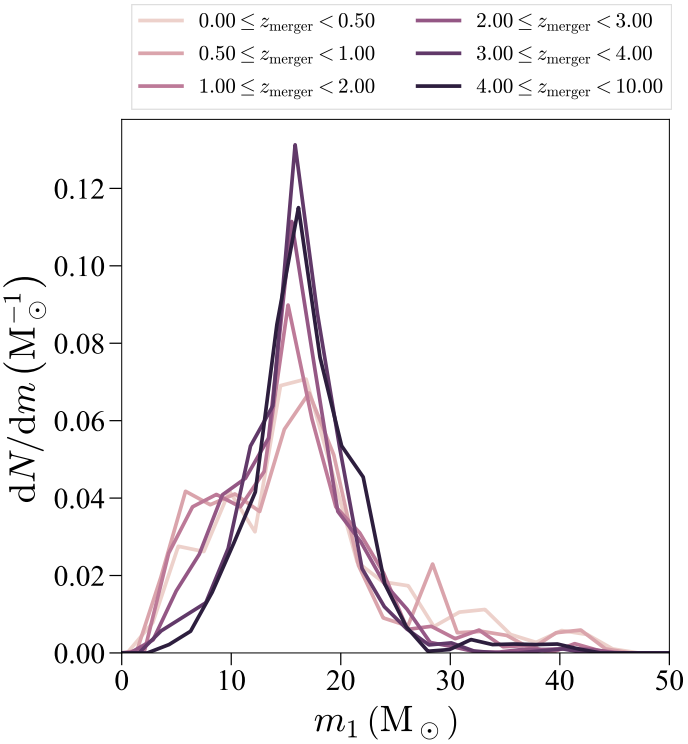

Figure 3. Primary mass distribution in BHBH mergers discriminated by $z_{\rm merger}$ in the Canonical model. The curves are normalized so that the are under each is unity. We find a dominant peak at $\sim 16\,\mathrm{M}_\odot$, but also a subdominant peak at $\sim 9\,\mathrm{M}_\odot$. Although the latter never becomes dominant, it shows a clear tendency to be populated at lower redshifts (particularly $\lesssim 2$); thus BHs with mass $\lesssim 12\,\mathrm{M}_\odot$ are more likely to merge at lower redshift. A small peak at $\sim 30\,\mathrm{M}_\odot$ is also found at lower redshifts and discussed in the text.

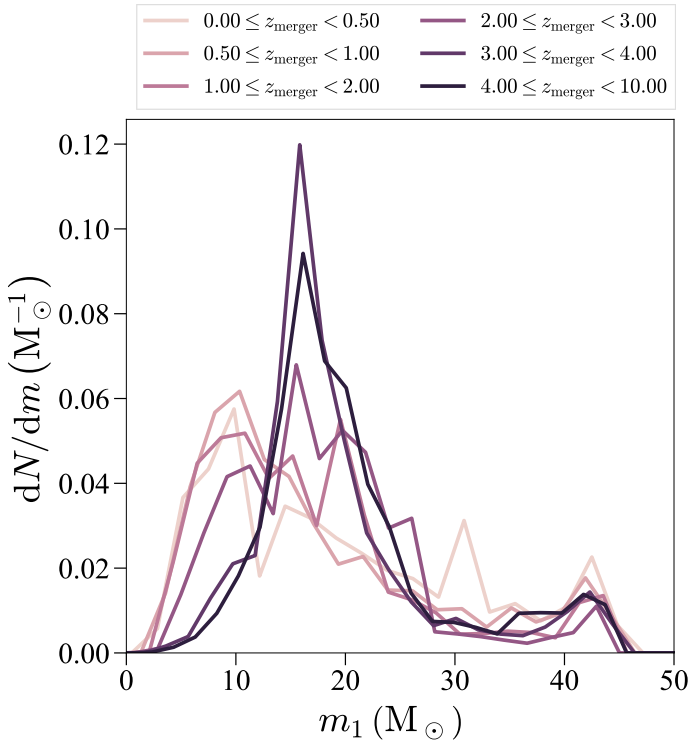

Figure 4. Same as Fig. 3 but for the IGIMF model, which amplifies the dependence of the masses on the redshift. In this case, the lower $\sim 9\,\mathrm{M}_\odot$ peak does become dominant for $z_{\rm merger} \lesssim 2$, while the $\sim 16\,\mathrm{M}_\odot$ remains dominant above $z_{\rm merger} \gtrsim 2$. The PPSINe $\sim 45\,\mathrm{M}_\odot$ is present at all redshift, and once again the $\sim 30\,\mathrm{M}_\odot$ peak appears at the lowest redshifts. In this case, there is a stronger trend for the more massive BHs to be merging at higher redshift, with $\sim 12\,\mathrm{M}_\odot$ serving as an approximate threshold for primary BHs merging below or above $z_{\rm merger} \sim 2$.

(2022a) employ the model by Farmer et al. (2019) for PPISNe, instead of Marchant et al. (2019); it remains for us to check whether the origin of the $\sim 30\,\mathrm{M}_\odot$ peak we find is also the transition between CCSNe and PPISNe, and why it appears only at low $z_{\rm merger}$.

Finally, we compute the time-evolution of the merger rates for all three classes of merger, as seen in Fig. 5 for both IGIMF and Canonical models. In general, the merger rates are characterized by an early peak in the $z_{\rm merger} \sim 1-4$ range, associated to the high SFR region in Fig. 2, followed by a smooth decrease down to $z_{\rm merger} = 0$. BHBH mergers peak earlier, followed by BHNSs and then NSNSs, the last of which are characterized by a stable rate after the peak. The IGIMF and Canonical models differ most strongly with regard to the position of the peaks and magnitude of the BHBH and BHNS merger rates. Both are associated with the peak in the top-heaviness of the varying IMF at $z \sim 2$ due to its SFR-dependence. In the Canonical model, the position of the peaks is set by a combination of the total amount of BCOs being formed, which increases with the size of the overall population for high SFRs; and the decreased efficiency of wind mass loss at low metallicities, which leads to a higher fraction of BCO progenitors at high redshifts. This tends to drag the peak up in redshift, until the point where the total population is too small to continue to increase the merger rate, even if the BCO fraction is large. In the IGIMF model, on the other hand, the top-heaviness of the IMF strongly amplifies the formation of BCO progenitors around $z_{\rm ZAMS} \sim 2$, which places the peak at later $z_{\rm merger}$. The top-heavy IMF also amplifies the formation of black hole progenitors more strongly than that of neutron star progenitors, such that, going from the Canonical to the IGIMF model, NSNS merger rates remain of the same order, but BHNS and BHBH rates increase by one order of magnitude.

Table 1. Local volumetric merger rates from both tested models, and the 90 % credibility intervals from GWTC-3 (Abbott et al. LIGO-Virgo-KAGRA Collaboration, 2021).

Source	Local merger rate ($\mathrm{Gpc}^{-3}\,\mathrm{yr}^{-1}$)		
	BHBH	BHNS	NSNS
IGIMF	94	68	8
Canonical	15	7	14
GWTC-3 (90%)	16 – 61	7.8 – 140	10 – 1700

However, neither of the models is fully compatible with the most recent 90% credibility intervals for local merger rates as inferred from GWTC-3 (Abbott et al. LIGO-Virgo-KAGRA Collaboration, 2021), as seen in Tab. 1. This is not surprising, as we have so far only tested two of the 192 possible permutations of our initial conditions models, and merger rates estimated from isolated binary evolution tend to be very sensitive to model choices (see Broekgaarden et al. (2021) for variations with regard to the evolution models in `COMPAS`, and Mandel & Broekgaarden (2022) for the full range of variations in the literature).

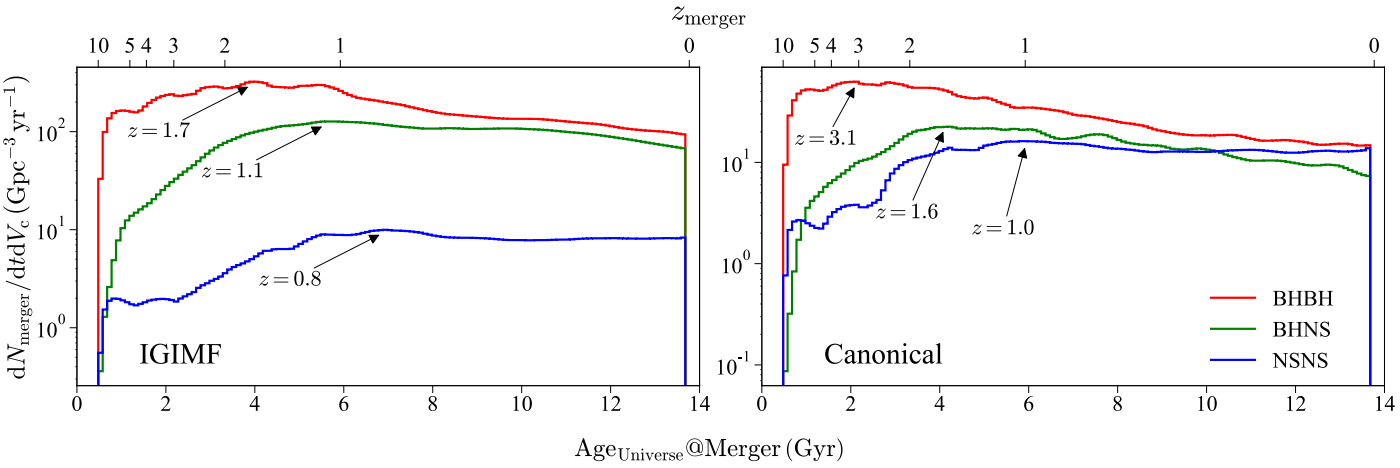

Figure 5. Merger rate time-evolution for all three merger classes, in both the IGIMF (left) and Canonical (right) models. All cases show a peak merger rate in the high SFR range ($z \sim 1-4$, see Fig. 2), followed by a smooth decrease down to $z_{\rm merger} = 0$. Relative to the Canonical model, the IGIMF model results in BHBH and BHNS rates one order of magnitude greater and in later peaks, both features connected to the top-heaviness of the IMF at high SFR. This amplifies both the total size of the population formed around the SFR peak ($z \sim 2$) and the fraction of black hole progenitors produced. A particularly significant consequence is that BHBH and BHNS mergers always remain dominant in the IGIMF case, while they become comparable to or subdominant with regard to NSNS mergers locally in the Canonical case. See text for further discussion.

4. Conclusions

We compared in this work the predictions for BCMs, in particular BHBH mergers, for two sets of initial condition models with the BPS code `COMPAS`: the Canonical model, with a Kroupa (2001) IMF and the typical distributions for orbital parameters (q from Sana et al. (2012), P from Öpik (1924) and $e = 0$); and the IGIMF model, with the metallicity- and SFR-dependent galaxy IMF from Jeřábková et al. (2018), and the correlated orbital parameter distributions from Moe & Di Stefano (2017). We build a composite binary population that reproduces the cosmic SFH between $z = 0$ and $z = 10$ based on Chruślińska, Nelemans & Belczynski (2019); Chruślińska et al. (2020).

We find that the IGIMF model leads to a strong dependece of the primary mass on redshift for BHBH mergers. While in the Canonical model a peak at $\sim 16\,\mathrm{M}_\odot$, associated with the CE channel, is always dominant, in the IGIMF model a lower peak at $\sim 9\,\mathrm{M}_\odot$, associated with the stable RLOF channel, dominates below $z_{\rm merger} \sim 2$. A small peak at $\sim 30\,\mathrm{M}_\odot$ for $z_{\rm merger} \lesssim 1$ might be associated to a similar feature found in the empirical distribution from GWTC-3, although it might also be a non-physical artifact of the transition between CCSNe and PPSINe regions. A further $\sim 45\,\mathrm{M}_\odot$ peak, with origin in stars undergoing PPISNe, is populated at all redshifts, but only in the IGIMF case.

Both models predict a peak in merger rates for BHBH, BHNS and NSNS binaries in the $z_{\rm merger} \sim 1-4$ range, associated to high SFRs and low metallcities. The additional top-heaviness of the variant IMF for high SFRs drags these peaks towards the lower end of this range in the IGIMF case. The IGIMF model results in merger rates one order of magnitude greater for BHBH and BHNS binaries overall; both models yield similar results for NSNS mergers. Locally, the IGIMF model predicts merger rates of 94, 68 and $8\,\mathrm{Gpc}^{-3}\,\mathrm{yr}^{-1}$; and the Canonical of 15, 7 and $14\,\mathrm{Gpc}^{-3}\,\mathrm{yr}^{-1}$, for BHBH, BHNS and NSNSs, respectively.

A presentation and discussion of the full set of results, as well a detailed description of our initial sampling pipeline, will be published in the near future as de Sá et al. (submitted). While neither model fully agrees with the most recent empirical constraints, we expect that a future exploration of the entire range of 192 possible initial condition permutations will result in a subset of models in better agreement with observations.

Acknowledgements. This research was funded by the FAPESP (São Paulo) grant number 2020/08518-2. L.M.S. acknowledges funding from the CNPq (Brazil), grant number 140794/2021-2. L.S.R was funded by the Capes (Brazil) and FAPESP grant number 2023/08649-8. J.E.H. has been partially supported by the CNPq. We thank Martyna Chruślińska for kindly providing their grid of IGIMF corrections for the SFR. Simulations in this paper made use of the `COMPAS` rapid binary population synthesis code (version 02.32.03), which is freely available at `http://github.com/TeamCOMPAS/COMPAS`.

References

Abbott et al. (LIGO-Virgo-KAGRA Collaboration) 2021, PRX, 13, 011048
Broekgaarden, F. S. et al. 2021, MNRAS, 508, 5028
Chruślińska, M., Nelemans, G. & Belczynski, K. 2019, MNRAS, 482, 5012
Chruślińska, M., Jeřábkov, r Nelemans, G. & Yan, Z. 2020, A& A, 636, A10
Farmer, R., Renzo, M., de Mink, S. E., Marchant, P. & Justham, S. 2019, ApJ, 887, 12
Fryer, C. L., Belczynski, K., Wiktorowicz, G., Dominik, M., Kalogera, V. & Holz, D. E. 2012, ApJ, 749, 14
Gunawardhana, M. L. P. et al. 2011, MNRAS, 415, 1647
Hopkins, A. M. 2018, PASA, 25, e039
Klencki, J., Moe, M., Gladysz, W., Chruslinska, M., Holz, D. E. & Belczynski, K., A& A, 619, 19
Jeřábková, T., Hasani Zonoozi, A., Kroupa, P., Beccari, G., Yan, Z., Vazdekis, A. & Zhang, Z.-Y. 2018, A& A, 620, A39
Kroupa, P. 2001, MNRAS, 322, 231
Kroupa, P. & C. Weidner 2003, ApJ, 598, 1076
Mandel, I. & Broekgaarden, F. S. 2022, Living Rev. Relativ., 25, 1
Marks, M., Kroupa, P., Dabringhausen, J. & Pawlowski, M. S. 2012, 422, 2246
Marchant, P., Renzo, M., Farmer, R., Pappas, K. M. W., Taam, R. E., de Mink, S. E. & Kalogera, V. 2019, 882, 17
Moe, M. & Di Stefano, R. 2017, ApJS, 230, 15
Öpik, E. 1924, Publications of the Tartu Astrofizica Observatory, 25, 1
Salpeter, E. E. 1955, ApJ, 121, 161
Sana, H., de Mink, S. E., de Koter, A., Langer, N., Evans, C. J., Gieles, M., Gosset, E., Izzard, R. G., Le Bouquin, J. B. & Schneider, F. R. N. 2012, Science, 337, 444
van Son, L. A. C., de Mink, S. E., Callister, T., Justham, S., Renzo, M., Wagg, T., Broekgaarden, F. S., Kummer, F., Pakmor, R. & Mandel, I. 2022, ApJ, 931, 17
van Son, L. A. C., de Mink, S. E., Renzo, M., Justham, S., Zapartas, E., Breivik, K., Callister, T., Farr, W. M. & Conroy, C. 2022, ApJ, 940, 17
Stevenson, S., Sampson, M., Powell, J., Vigna-Gómez, A., Neijssel, C. J., Szécsi, D. & Mandel, I. 2019, ApJ, 882, 15
Team COMPAS: Riley, J. et al. 2022, ApJS, 258, 34